Efficiency limits of Si/SiO_2 quantum well solar cells from first-principles calculations

Thomas Kirchartz, Kaori Seino, Jan-Martin Wagner, Uwe Rau, and Friedhelm Bechstedt

Citation: Journal of Applied Physics **105**, 104511 (2009);
View online: https://doi.org/10.1063/1.3132093
View Table of Contents: http://aip.scitation.org/toc/jap/105/10
Published by the American Institute of Physics

Efficiency limits of Si/SiO_2 quantum well solar cells from first-principles calculations

Thomas Kirchartz,[1,a)] Kaori Seino,[2] Jan-Martin Wagner,[2,b)] Uwe Rau,[1] and Friedhelm Bechstedt[2]
[1]*IEF5-Photovoltaik, Forschungszentrum Jülich, 52425 Jülich, Germany*
[2]*Institut für Festkörpertheorie und-optik, Friedrich-Schiller-Universität Jena, Max-Wien-Platz 1, 07743 Jena, Germany*

(Received 9 February 2009; accepted 15 April 2009; published online 26 May 2009)

In order to investigate the applicability of new photovoltaic absorber materials, we show how to use first-principles calculations combined with device simulations to determine the efficiency limits of solar cells made from SiO_2/Si superlattices and from coaxial ZnO/ZnS nanowires. Efficiency limits are calculated for ideal systems according to the Shockley–Queisser theory but also for more realistic devices with finite mobilities, nonradiative lifetimes, and absorption coefficients. Thereby, we identify the critical values for mobility and lifetime that are required for efficient single junction as well as tandem solar cells. © *2009 American Institute of Physics*. [DOI: 10.1063/1.3132093]

I. INTRODUCTION

Since the early days of solar cell research, the focus has been on a rather small number of materials, such as amorphous[1] and crystalline[2] silicon or the quaternary system $Cu(In,Ga)(Se,S)_2$.[3,4] The research process was basically "bottom up," i.e., the main task of theoretical work was to explain the experimental findings. Meanwhile, being now a much more mature field,[5] research is also driven by abstract ideas and novel concepts,[6–9] promising to overcome the classical efficiency limit of Shockley and Queisser[10] (SQ limit). Research is now partly "top down" meaning that theoretical considerations and calculations[11] will first estimate the potential of a concept, which is then pursued experimentally.

Theoretical calculations for estimation of efficiency limits of a given material are a two step process. The first step needs to derive material parameters theoretically. This task may be realized for instance by first-principles calculations or calculations via the effective-mass approximation (EMA)[12–14] that determines the band structure of the new material. From this band structure, quantities such as absorption coefficient and density of states follow, which subsequently serve to evaluate the efficiency limits of the given material. A first estimate of efficiency directly follows from the band gap, by calculating the SQ limit. However, with this approach a high amount of information contained e.g., in the absorption coefficient is lost.[15]

This paper therefore shows how to go step by step from the SQ limit to realistic efficiencies. Thereby, we are able to identify both the potential of a given concept and also the critical order of magnitude required of those parameters that are not accessible by first-principles calculations. For example, we show how to determine the necessary thickness and the necessary quality of the light trapping scheme to have enough absorption of photons. We also estimate the mobilities and lifetimes necessary for efficient extraction of carriers and a sufficiently high open circuit voltage.

As depicted in Fig. 1, the materials we investigate are SiO_2/Si quantum wells,[16] which we compare to recently published theoretical data[17] on coaxial ZnO/ZnS nanowires. These materials have in common that they are all possible candidates as the high band gap partner in a tandem configuration, for instance with crystalline silicon, and that the materials are abundant and nontoxic. Finding materials with high band gaps $E_g \approx 1.7-1.9$ eV as a tandem partner is probably the most feasible way to enhance current state of the art single junction concepts *considerably* above their present limits. This is because up to now multijunction approaches are the only concept that has proven its ability to increase efficiencies above the SQ limit.[18,19] All other concepts, such as up[20,21] and down conversion,[22,23] hot carrier solar cells,[24–26] and multiple exciton generating absorbers[27–33] are still lacking experimental proof for efficiencies above the SQ limit.

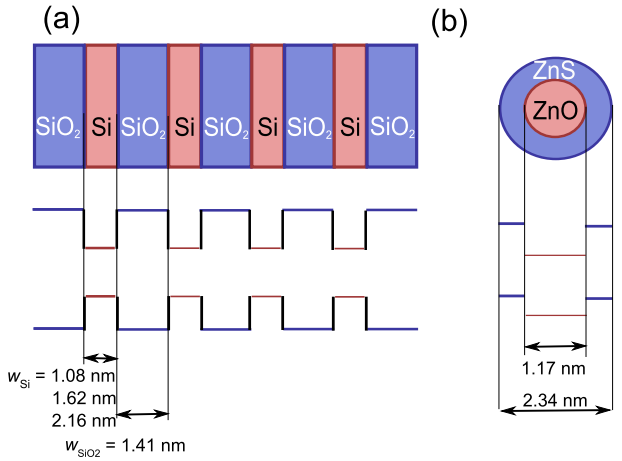

FIG. 1. (Color online) Scheme of the two investigated materials, (a) a SiO_2/Si superlattice and (b) a ZnO/ZnS nanowire. For both materials the schematic band diagram and the thicknesses and diameters of the geometry are given.

[a)]Electronic mail: t.kirchartz@fz-juelich.de.
[b)]Present address: Max-Planck-Institut für Mikrostrukturphysik, Weinberg 2, 06120 Halle, Germany.

A natural candidate as a tandem partner for single junction cells with band gaps around $E_g \approx 1.1$ eV would be amorphous silicon.[34] However, although it has an adequate band gap of around 1.8 eV, amorphous silicon is currently lacking a sufficiently high short circuit current to make current matching with high quality solar cells like *c*-Si possible. Therefore, superlattice absorber materials using SiO_2/Si,[35–39] SiN_x/Si,[40] or SiC/Si[41,42] quantum wells or quantum dots are currently investigated experimentally by different research groups. Deposition of such stacks is possible, for instance, with plasma enhanced chemical vapor deposition of alternating layers of Si and SiO_2 followed by a rapid thermal annealing step. Confinement effects[43] in the superlattices allow band gaps to be adjusted by changing the thickness of the Si layer and the thickness and material of the surrounding dielectric. In addition, the small size of these quantum confinement structures is supposed to lead to increased oscillator strength. However, quantum confinement is in contrast to the task of charge carrier extraction, requiring highly mobile carriers. In addition, a quantum confinement implies an increase in internal interface area, which is most likely to be detrimental for nonradiative charge carrier lifetimes. Thus, the main challenge for any absorber making use of quantum effects is the achievement of sufficiently high absorption at the right band gap–for example for use in tandem configuration with *c*-Si–but at the same time the achievement of high carrier mobilities[44] and carrier lifetimes albeit the large band offsets and the many interfaces in the absorber.

II. THEORY

A. First-principles calculations

The electronic and optical properties of the Si/SiO_2 and ZnO/ZnS quantum structures as well as the underlying atomic geometries are modeled in the framework of the *ab initio* density functional theory (DFT) where the exchange and correlation effects are included within the local density approximation (LDA). For details the reader is referred to the papers by Seino *et al.*[16] and Schrier *et al.*[17] In the case of the Si/SiO_2 multiquantum-well (MQW) structures we use the DFT as implemented in the Vienna *Ab initio* Simulation Package.[45] The all-electron wave functions and the pseudopotentials for the electron-ion interaction are described within the projector-augmented wave method.[46] Plane waves up to a kinetic-energy cutoff of 30 Ry give converged results for the silicon dioxide[47] and hence also for the Si/SiO_2 structures. The Brillouin-zone (BZ) integrations in the computations of the total energy, the electron density, the density of states (DOS), and the dielectric function are replaced by summations over equally distributed Monkhorst–Pack **k**-points, where **k** is the wave vector. Their convergence is tested for each quantity separately.

The atomic geometries are considered to be in equilibrium when the Hellmann–Feynman forces are smaller than 10 meV/Å. The total-energy minimization procedures lead to theoretical cubic lattice constants of diamond Si and β-cristobalite SiO_2 of $a_0 = 5.40$ Å and 7.39 Å, respectively.[47] As shown in Fig. 1 we use Si-layer thicknesses $w_{Si} = 1.08$, 1.62, and 2.16 nm, i.e., of two, three, or four primitive unit cells, in order to vary the strength of the electron and hole confinement. The SiO_2 barrier layer thickness is fixed at about two unit cell extents. Smaller values reduce the confinement, while thicker layers do not influence it. Including a slight biaxial strain in the SiO_2 layers of the [001]-oriented MQW system in order to make their in-plane lattice constant fit to the diagonal of the bulk Si (001) surface unit cell, this leads to an effective layer thickness of $w_{SiO_2} = 1.41$ nm.

Each SiO_2/Si interface contains two dangling bonds (DBs) per $(\sqrt{2} \times \sqrt{2})R45°$ Si lateral unit cell. Different passivations of the DBs or reconstructions result in various interface models that can be used in the calculations. Recently we studied at least four such models.[16,48] Here, we focus our attention on the most likely interface element. The Si interface atom not being bonded to the SiO_2 is replaced by an oxygen atom forming a Si–O–Si bond. This is the so-called bridge-oxygen model for the $SiO_2/Si(001)$ interface.[49]

The Kohn–Sham equation of the DFT-LDA yields eigenvalues $E_\nu(\mathbf{k})$ and eigenfunctions $\psi_{\nu\mathbf{k}}(\mathbf{x})$ of the studied quantum structure, here of the studied $SiO_2/Si(001)$ superlattice. Thereby, the band index ν runs over all (empty) electron subbands, the conduction bands *C*, as well as all (occupied) hole subbands, the valence bands *V*. The wave vector **k** varies within the flat BZ of the superlattice structure. In the ground-state theory DFT the excitation aspect, i.e., the appearance of electrons and holes, more strictly, quasielectrons and quasiholes, is missing. This deficiency leads to a significant underestimation of the band gaps and optical transition energies,[50] which can be corrected within the quasiparticle (QP) theory. Using the QP theory fundamental band gaps are comparable with the measured values and the results for the calculation with the QP theory show a much better agreement with experiment than the DFT-LDA results for SiO_2/Si superlattices.[16] Here, we use a scissors operator approach to account for the band gap underestimation and widen correspondingly the distance of empty and occupied states $E_C(\mathbf{k}) - E_V(\mathbf{k}) + \Delta$. The value Δ depends on the confinement.[51] Consequently, we use for the imaginary part of the dielectric function $\varepsilon_\alpha(\omega)$ the result of the independent QP approximation,[52]

$$\mathrm{Im}\ \varepsilon_\alpha(\omega) = 8\left(\frac{\pi q}{m_0 \omega}\right)^2 \frac{1}{\Omega} \sum_{\mathbf{k}} \sum_{C,V} |\langle \psi_{C\mathbf{k}} | p_\alpha | \psi_{V\mathbf{k}} \rangle|^2 \delta(E_C(\mathbf{k}) - E_V(\mathbf{k}) + \Delta - \hbar\omega) \quad (1)$$

with the angular frequency ω, the elementary charge q, the cell volume Ω, and the Cartesian direction α of the light polarization. Then, one has for the single QP DOS,

$$D(E) = \frac{2}{\Omega} \sum_{\mathbf{k}} \sum_{\nu} \delta[E_\nu(\mathbf{k}) + \delta_{\nu C}\Delta - E]. \quad (2)$$

The quantum confinement effects in the Si layers of the $SiO_2/Si(001)$ MQW structures lead to a drastic redistribution of the electronic states. The first direct gap with a small but finite oscillator strength occurs much below the bulk E_0 transition energy of about 3.1 eV. This symmetry break of the **k**-selection rule has enormous consequences for the absorption coefficient $\alpha(E)$ derived from the dielectric function (1). However, besides the light absorption coefficient and there-

fore the role of the electron-hole pair generation, the efficiency of a solar cell is dominated by the mobility of the electrons and holes. Usually these mobilities are calculated within the EMA.[12–14]

This approximation is however not anymore valid for a superlattice with extremely small layer thicknesses w_{Si} and w_{SiO_2}. The confinement leads to many electron and hole subbands, which are all involved in the transport processes.[16] Moreover, the subbands in the main transport direction parallel to the superlattice axis are rather flat and hence have to be described by typical carrier masses larger than the free electron mass m_0 due to the low tunneling efficiency for the SiO_2 barriers. Therefore, similarly to the bulk Si case we study the effective density of states (where k denotes Boltzmann's constant and T the absolute temperature),

$$N_C = \int_{E_{CBM}}^{\infty} dE \exp\left(-\frac{E - E_{CBM}}{kT}\right) D(E),$$

$$N_V = \int_{-\infty}^{E_{VBM}} dE \exp\left(-\frac{E_{VBM} - E}{kT}\right) D(E) \quad (3)$$

for nondegenerate carrier gases at room temperature $kT = 25$ meV. For the electrons (holes) the effective DOS N_C (N_V) is limited by the lowest conduction subband energy E_{CBM} (highest valence subband energy E_{VBM}) and the single QP DOS (2). The effective DOSs describe the carriers distributed by an exponential weight over the corresponding subbands. They correspond to quantities averaged also over all directions. In the bulk case with an isotropic electron (hole) effective mass m_n (m_p) expression (3) yields,[13,14]

$$N_C = \frac{1}{4\pi^3}\left(\frac{2\pi m_n kT}{\hbar^2}\right)^{3/2},$$

$$N_V = \frac{1}{4\pi^3}\left(\frac{2\pi m_p kT}{\hbar^2}\right)^{3/2}, \quad (4)$$

where $\hbar$ is Planck's constant h divided by 2π. However, the resulting effective masses are characteristic for carrier motion in all space directions. For a solar cell with n- and p-contacts at the bottom and the top of the SiO_2/Si superlattice, one may assume that only the effective averaged carrier masses for the direction perpendicular to the SiO_2/Si interfaces may be relevant. In this case we neglect the motion parallel to SiO_2/Si interfaces and restrict expressions (3) and (4) to the one-dimensional (1D) case. Then, taking into account the definition of the DOS,[13,14] the 1D effective DOS reads as

$$N_C^{1D} = \frac{2}{w_{Si} + w_{SiO_2}} \sum_C \frac{1}{N_{k_z}} \sum_{k_z} \exp\left(-\frac{E_C(k_z) - E_{CBM}}{kT}\right),$$

$$N_V^{1D} = \frac{2}{w_{Si} + w_{SiO_2}} \sum_V \frac{1}{N_{k_z}} \sum_{k_z} \exp\left(-\frac{E_{VBM} - E_V(k_z)}{kT}\right), \quad (5)$$

with N_{k_z} as the number of k_z-points chosen along the superlattice axis and $E_\nu(k_z)$ as the subband dispersion. For single parabolic bands in 1D one finds

$$N_C^{1D} = \frac{1}{\pi}\left(\frac{2\pi m_n^{1D} kT}{\hbar^2}\right)^{1/2},$$

$$N_V^{1D} = \frac{1}{\pi}\left(\frac{2\pi m_p^{1D} kT}{\hbar^2}\right)^{1/2}. \quad (6)$$

Relation (6) allows us to define 1D effective electron and hole masses, which are characteristic for the tunneling through the SiO_2 barriers.

B. Shockley–Queisser limit–optical calculations

The most basic requirement for any photovoltaic absorber material is that it absorbs light in an appropriate range of photon energies. For nonconcentrating terrestrial outdoor applications, the standard sun spectrum defining what is the "appropriate" range of photon energies is the AM1.5G spectrum ϕ_{sun}. To calculate the photon flux that is absorbed by a semiconductor, we need to know its absorptance in addition to the spectrum of incoming photons. To determine the exact absorptance $a(E)$ of a given sample, it is necessary to know the absorption coefficient α, index of refraction n, the optical properties of surfaces, and interfaces as well as the thickness d. However, on a slightly higher level of abstraction, the best possible isotropic absorptance $a(E)$ is only characterized by a single quantity, the band gap E_g. The ideal absorptance is then defined as zero below the band gap and one above the band gap. The photocurrent in the SQ limit is then

$$J_{sc,SQ} = q\int_0^{\infty} a(E)\phi_{sun}(E)dE = q\int_{E_g}^{\infty} \phi_{sun}(E)dE. \quad (7)$$

The photocurrent however is not sufficient to calculate the power conversion efficiency of a solar cell. We also need the recombination current, which—in the SQ limit—only depends on the photon flux emitted by the solar cell. Since the SQ limit assumes perfect transport of carriers, i.e., flat quasi-Fermi levels, the application of a voltage V to the junction of the solar cell leads to an excess emission of photons given by[53]

$$\phi_{em}(E) = a(E)\phi_{bb}(E)\left[\exp\left(\frac{qV}{kT}\right) - 1\right]. \quad (8)$$

The spectral dependence of the black body radiation emitted into the half sphere above the solar cell is given by[54]

$$\phi_{bb}(E) = \frac{2\pi E^2}{h^3c^2}\frac{1}{[\exp(E/kT) - 1]} \approx \frac{2\pi E^2}{h^3c^2}\exp\left(\frac{-E}{kT}\right), \quad (9)$$

where c is the vacuum speed of light. Equation (8) directly follows from Kirchhoff's law,[55] stating that absorptance and emissivity of a body are equal for each energy and spherical angle.

The photon flux ϕ_{em} emitted by the solar cell must originate from a recombination current $J_{rec,SQ} = q\int\phi_{em}dE$. If we separate the prefactor from the exponential term in Eq. (8), the saturation current density $J_{0,SQ} = J_{rec,SQ}/[\exp(qV/kT)-1]$ follows as,

$$J_{0,\mathrm{SQ}} = q\int_0^\infty a(E)\phi_{\mathrm{bb}}(E)dE = q\int_{E_g}^\infty \phi_{\mathrm{bb}}(E)dE \tag{10}$$

and the total current/voltage (J/V) curve of the solar cell is given by

$$J = J_{0,\mathrm{SQ}}\left[\exp\left(\frac{qV}{kT}\right) - 1\right] - J_{\mathrm{sc,SQ}}. \tag{11}$$

From this J/V curve, the efficiency follows as the electrical power density $P=J_{\mathrm{mp}}V_{\mathrm{mp}}$ at maximum power point $(J_{\mathrm{mp}}, V_{\mathrm{mp}})$ relative to the incoming optical power density. Using step-functionlike absorber profiles Eqs. (7)–(11) allow the calculation of the efficiency of single- and multijunction solar cells as a function of band gap.[56,57]

Using the band gap as the only parameter to describe optical properties of a device, however, implies a loss of information if the absorption coefficient of a certain material is already known. It is of course possible to calculate the SQ limit also for non step-functionlike absorptances, which merely requires ignoring the simplification on the right hand side of Eqs. (7) and (10). To calculate these absorptances, one needs to agree on a reasonable upper limit for the absorptance of a given material. The absorptance always depends on the thickness of the absorber layer, which is therefore the only quantity that has to be chosen arbitrarily. The absorptance also depends on the optical properties of the solar cell. A very rough surface acting as a diffuser for the light will usually enhance the optical absorption by increasing the number of oblique paths through the absorber, thereby increasing the pathlength and the probability of total internal reflection.[58–60] A reasonable ideal case for the absorptance is the one where the light is scattered isotropically, thereby creating a Lambertian light distribution inside the absorber.[61] The absorptance for Lambertian scattering is the perfect case for isotropic illumination; only for tracked systems, where the light comes always from the same solid angle, better light trapping and higher absorptances are possible.[62]

To calculate the absorptance, we assume a front surface reflectance $R_f=0$ and a back surface reflectance $R_b=1$ as well as one Lambertian diffuser on top of the absorber layer. Then the absorptance follows as,[63–65]

$$a(E) = \int_0^d 2\alpha(E)(1-R_f)\frac{Ei_2(\alpha(E)x) + Ei_2(\alpha(E)(2d-x))}{1 - t_{\mathrm{cell}}(E)(1-t_{\mathrm{lamb}})}dx, \tag{12}$$

with $t_{\mathrm{lamb}}=1/n^2$, n the index of refraction. Equation (12) uses the definition

$$t_{\mathrm{cell}}(E) = e^{-2\alpha(E)d}[1-2\alpha(E)d] + [2\alpha(E)d]^2 Ei[2\alpha(E)d] \tag{13}$$

for the angle-integrated transmission of the cell from the front with one reflection at the back side to the front, where

$$Ei(z) := \int_z^\infty \frac{e^{-t}}{t}dt \tag{14}$$

is the exponential integral, and

$$Ei_2(z) := z\int_z^\infty \frac{e^{-t}}{t^2}dt = e^{-z} - zEi(z). \tag{15}$$

C. Detailed balance model for pin-type solar cells

Not only imperfect absorption but also insufficient carrier collection due to low mobilities can be included in a detailed balance model. The term "detailed balance model" is frequently used in context with the SQ limit, which bases on the detailed balance between incoming and outgoing photon fluxes. However, detailed balance is much more general, meaning that in thermodynamic equilibrium any process is exactly counterbalanced by its inverse process.[66–72] The SQ limit relies on one detailed balance pair only, namely, photogeneration and radiative recombination leading to the situation that in thermodynamic equilibrium the absorbed photon flux and the emitted photon flux are the same, namely, $a(E)\phi_{\mathrm{bb}}(E)$. If one extends the concept of detailed balance to any process in the device, it is possible to design a model for solar cells with finite mobilities that is compatible to the SQ limit in the sense that, when the carrier mobilities are high enough to warrant perfect collection, the results are the same. One feature a model has to have, to ensure compatibility with SQ, is the inclusion of photon recycling, i.e., the generation of electron/hole pairs by photons emitted from the device itself.[73]

A detailed balance model including photon recycling was already developed by Mattheis *et al.*,[74] however it was restricted to *pn*-junction solar cells in low level injection (only minority carriers are considered). For thin film solar cells with low mobilities, usually pin-junction devices are preferred due to better charge carrier extraction.

To calculate the carrier concentrations as a function of depth in the absorber, three differential equations have to be solved: the Poisson equation, $\Delta\varphi=-\rho/\varepsilon$ (relating the electrical potential φ to the space charge ρ and the dielectric constant ε), and the continuity equations describing transport as well as generation and recombination of carriers. The drift-diffusion equations for the electron concentration n and the hole concentration p in a pin-type device are given by

$$-\frac{1}{q}\frac{dJ_n}{dx} = -D_n\frac{d^2n}{dx^2} - F\mu_n\frac{dn}{dx} = g - R_{\mathrm{rad}}np, \tag{16}$$

$$\frac{1}{q}\frac{dJ_p}{dx} = -D_p\frac{d^2p}{dx^2} + F\mu_p\frac{dp}{dx} = g - R_{\mathrm{rad}}np, \tag{17}$$

where J_n and J_p are the electron and the hole current densities, F is the electric field strength, g the generation rate, $D_{n,p}=\mu_{n,p}kT/q$ is the diffusion constant of the electrons and holes, which depends on the electron and hole mobilities μ_n and μ_p and on the thermal voltage kT/q. Due to the principle of detailed balance, the radiative recombination constant R_{rad}

is linked to absorption via the van Roosbroeck–Shockley equation,[75]

$$R_{\mathrm{rad}} n_i^2 = \int \alpha(E)\phi_{\mathrm{bb}}(E)dE, \tag{18}$$

where n_i is the intrinsic carrier concentration.

The intrinsic carrier concentration has different impacts on device performance. A high intrinsic carrier concentration increases the number of carriers available for transport. Thus, the critical mobility, where the short circuit current decreases drastically due to insufficient transport, is shifted toward lower values. However, a high intrinsic carrier concentration also increases the radiative and nonradiative recombination current at a given quasi-Fermi level splitting since it increases the number of free carriers that can recombine. Thus a high intrinsic carrier concentration decreases the open circuit voltage.

At this point it is necessary to hint at some apparent contradiction. It might seem that in the radiative limit, the intrinsic carrier concentration should not play a role, since we did not have to assume a value for n_i in the corresponding Eqs. (7)–(15). Only the absorptance sufficed to determine the high mobility limit. The key to this is the van Roosbroeck–Shockley Eq. (18). Absorption coefficient and black body spectrum fix the product of n_i^2 and the radiative recombination rate. That means the intuitive assumption that a lower band gap leads to a lower open circuit voltage if everything else is kept the same can be understood by considering both sides of Eq. (18). Either one understands that an increase in the left hand side by a decrease in E_g and a subsequent increase in n_i leads to more recombination and a smaller open circuit voltage. Or one considers that a shift of the maximum of $\alpha\phi_{\mathrm{bb}}$ leads to a strong increase in the integral on the right hand side, since the black body spectrum increases exponentially with decreasing energy. While the calculation of the recombination rate from the radiative emission [right hand side of Eq. (18)] is only possible in the radiative limit, the argumentation that a high n_i leads to a high recombination current when the minority carrier lifetimes are kept constant stays the same also for nonradiative recombination.

Figure 2 shows the schematic band diagram of the pin-type solar cell under investigation. We only solve the continuity equations in the intrinsic region, while the *p*- and the *n*-type layer are assumed to be infinitely thin and serve only as the boundary condition. In general, we need four extraction/injection velocities at the two contacts, i.e., two at $x=0$ and two at $x=d$. For simplicity, we assume throughout the paper that the electron contact is only active for electrons and hole contact is only active for holes, meaning that surface recombination of minorities is suppressed. Thus, we have two boundary conditions left. For the electrons at the electron collecting contact ($x=0$), we consider the possibility of extraction and injection to obtain a net electron particle current density,

$$j_n = S_n^* n_j - S_n n_b, \tag{19}$$

where the rate constants S_n, S_n^* have the dimension of a (collection or injection) velocity. Note that particle current densities are denoted as j, while electrical current densities are denoted as $J=qj$. In Eq. (19), the concentration of electrons on the bulk side of the contact is denoted as $n_b(x=0^+)$ and the concentration of electrons on the contact side is denoted $n_j(x=0^-)$. Detailed balance requires now that the net current is zero in thermodynamic equilibrium, thereby interlinking the two rate constants via

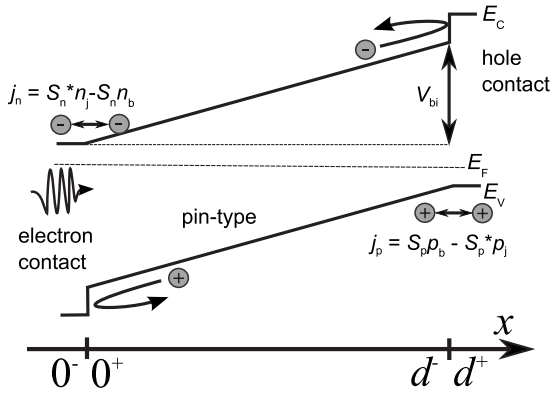

FIG. 2. Schematic band diagram of the simulated pin-type solar cell highlighting the boundary conditions needed for the model in Sec. II C. At the electron contact at $x=0$, we allow for electron extraction and injection, while the extraction of holes, which corresponds to the recombination of holes, is set to zero. At the hole contact, at $x=d$, the difference between hole extraction and injection gives the net hole current. Again, minority carrier recombination is set to zero.

$$S_n^* n_{j0} = S_n n_{b0}, \tag{20}$$

where $n_{b/j0}$ is the equilibrium concentration of electrons in the bulk/junction. Equivalently, for the holes at the hole contact ($x=d$) holds

$$j_p = -S_p^* p_j + S_p p_b \tag{21}$$

with

$$S_p^* p_{j0} = S_p p_{b0}. \tag{22}$$

In the simulations, we choose the collection and injection velocities $S_{n,p}$ for the majorities such that collection and injection is not current limiting. This is achieved for $S_{n,p} = 10^{10}$ cm/s, which is therefore a good approximation to infinity. In addition to the boundary conditions for the two types of carriers, we have to define boundary conditions for the electrical potential φ. In contrast to *pn*-junction solar cells, where applying a forward voltage means to inject minority carriers at the *pn*-junction into the base, in pin-junctions, electrons are injected into the intrinsic layer at the *n*-contact and holes at the *p*-contact. This is achieved by changing the potential between the electron and hole contact via

$$V_{\mathrm{bi}} = V_{\mathrm{bi},0} - V, \tag{23}$$

where V is the applied voltage and $V_{\mathrm{bi},0}$ is the equilibrium built-in voltage.

III. RESULTS

A. Optical limits

From the first-principles calculations, we derived absorption coefficients, effective DOSs, and anisotropic effec-

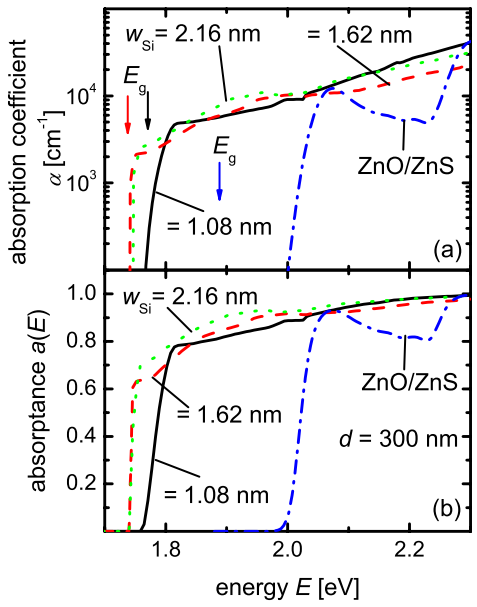

FIG. 3. (Color online) (a) Absorption coefficient and (b) absorptance of the three SiO_2/Si quantum wells and of the ZnO/ZnS nanowire. For the absorptance, we assumed a thickness of $d=300$ nm, Lambertian light trapping, and zero front surface reflection as well as unity back surface reflection.

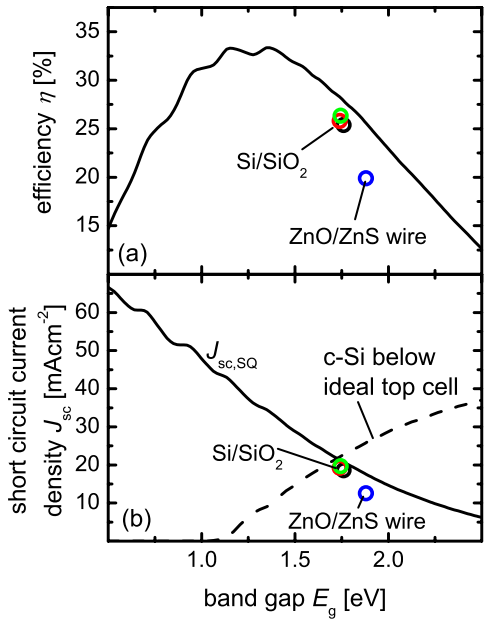

FIG. 4. (Color online) (a) Efficiency as a function of band gap for step-functionlike absorptances (solid line), an absorber temperature $T=300$ K, and an AM1.5G spectrum. The radiative high mobility efficiencies of the three SiO_2/Si quantum well configurations and of the ZnO/ZnS nanowire are indicated by open symbols. The thickness of the Si layer is $w_{Si}=2.16$, 1.62, and 1.08 nm from high efficiency to low efficiency. (b) Short circuit current density in the SQ limit as a function of band gap (solid line) and short circuit current density of a 200 μm thick c-Si solar cell in the high mobility limit and with Lambertian light trapping (dashed line). The c-Si cell is assumed to be optically below an ideal step-functionlike top cell with the band gap indicated by the x-axis. Thus, the intersection of the dashed and the solid line marks band gap and efficiency of the perfect top cell for c-Si. The short circuit current of the SiO_2/Si quantum well configurations and of the ZnO/ZnS nanowire is again indicated by open symbols.

tive masses in transport direction. In a first step, we focus only on the optical properties of our materials, i.e., on the absorption coefficient and the index of refraction.

In the original SQ theory, the radiative limits of solar cells were calculated only from the band gap, assuming a step-functionlike absorptance. However, in reality the cells will have a finite thickness and the absorptance will be smeared out at the band gap. The information about increased oscillator strengths and therefore increased absorption coefficients will be lost by discussing only infinitely thick absorbers. Thus, we need to calculate the radiative limit for finite thicknesses, which requires that we agree on a certain thickness of the absorber layers. For the moment, we choose a thickness $d=300$ nm, which is typical for other thin film approaches like amorphous silicon. Later, we will also discuss the thickness dependence of the photocurrent.

Equation (12) allows the calculation of the absorptances from the absorption coefficients in the limit of Lambertian light trapping. One additional requirement for the calculation of the absorptances is the knowledge of the refractive index n of the absorber material. This is due to the fact that the product of photon DOS and speed of light in a medium with refractive index n scales with n^2. Isotropically distributed photons will always have a higher density in the medium compared to air or vacuum and thus also the path length of weakly absorbed photons scales with n^2. Total internal reflection described by Snell's law guarantees that this thermodynamic requirement actually holds, by defining the transmission through a Lambertian surface as $t_{lamb}=1/n^2$ [see Eq. (12)]. The refractive indices n_{SL} used for calculation of the absorptances of the SiO_2/Si superlattices are estimated from the empirical refractive indices of Si and SiO_2 via

$$n_{SL}=\frac{w_{Si}n_{Si}+w_{SiO_2}n_{SiO_2}}{w_{Si}+w_{SiO_2}}. \tag{24}$$

For the refractive index of silicon and SiO_2 we used $n_{Si}=3.5$ and $n_{SiO_2}=1.5$ leading to the values $n_{1.08}=2.37$, $n_{1.62}=2.57$, and $n_{2.16}=2.71$ for the refractive indices for the cells with $w_{Si}=1.08$, 1.62, and 2.16 nm, respectively. The refractive index n_{nw} of the ZnO/ZnS nanowire is simply unknown. Even the assumption that it may be in between the refractive indices for ZnO and ZnS seems not to be valid in this case of a type II heterojunction. The band gap of the nanowires is not in between the band gap of ZnO and ZnS but much lower, meaning that the optical properties of the nanowire are fundamentally different from either of the two bulk materials. In order to avoid big differences compared to the superlattices that are due to this unknown refractive index, we choose it to be $n_{nw}=2.5$.

With the help of the refractive indices defined above and the absorption coefficients calculated from first principles and presented in Fig. 3(a), Eqs. (12)–(15) allow the calculation of the absorptances [see Fig. 3(b)]. Equations (7)–(11) then allow us to calculate the radiative high mobility efficiencies of the three SiO_2/Si quantum well configurations and of the ZnO/ZnS nanowire. Figure 4(a) compares these radiative efficiencies (open circles) with the result of the SQ theory (solid line). Figure 4(b) presents the corresponding

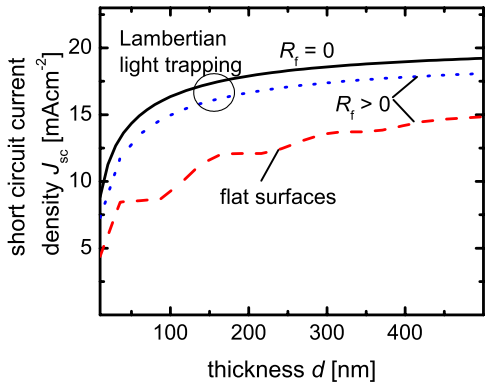

FIG. 5. (Color online) Short circuit current density displayed as a function of absorber thickness in the high mobility limit for the SiO_2/Si quantum well configuration ($w_{Si}=1.08$ nm) for Lambertian light trapping with perfect antireflective coating, i.e., $R_f=0$ (lines), for Lambertian light trapping and considering the reflections at an air/glass and glass/ZnO interface, i.e., $R_f>0$ (dotted lines) and for flat surfaces (dashed line) where the same finite reflection at the front is included as for the dotted line. In case of the flat surfaces, the simulation includes coherent interference in all layers except the front glass. The difference between the flat surface (dashed line) and the Lambertian surface (dotted line) due to light trapping is tremendous, namely, around 4 mA/cm^2 at $d=300$ nm, showing the large influence of light trapping for these thin devices.

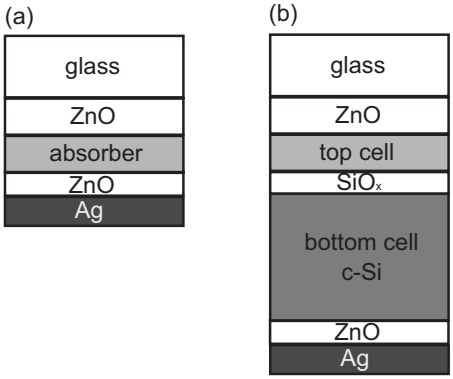

FIG. 6. Scheme of the layer stacks used for the calculation of the efficiencies with nonradiative recombination. The stack shown in (a) is used for Fig. 5 (dashed and dotted line) and Fig. 10, while the tandem cell in (b) is used for Fig. 11. The absorber layer in (a) and the top cell in (b) represents the superlattice or nanowire layer.

short circuit current densities, again in comparison to the SQ theory. In addition to the short circuit current densities in the SQ limit and the radiative limit of the four cells with finite thicknesses, the dashed line represents the short circuit current density of a 200 μm thick silicon cell, again with Lambertian light trapping, that is placed optically below a step-functionlike top cell with the band gap as indicated by the x-axis. That means, for a two-terminal tandem configuration with a very good crystalline silicon cell as the bottom cell, the intersection of dashed and solid line defines the perfect band gap and the short circuit current to be achieved. The values of this intercept are $E_g=1.72$ eV and $J_{sc}=21.7$ mA/cm^2. The values of the three SiO_2/Si superlattices are quite close to this intersection, while the ZnO/ZnS nanowire has a slightly too high band gap and too low short circuit current, meaning that it would require a higher band gap bottom cell or a triple junction configuration for best performance.

The calculations in Figs. 3 and 4 have been performed assuming a thickness $d=300$ nm, which is typical for other thin film solar cells like amorphous silicon. In the following, we will briefly discuss the influence of absorber layer thickness and optical properties of the interfaces on the photogenerated current. Thus, Fig. 5 shows the evolution of short circuit current density J_{sc} versus absorber thickness for one of the three SiO_2/Si superlattices ($w_{Si}=1.08$ nm). The lines correspond to the absorptance calculated with Eq. (12) under the assumption of Lambertian light trapping.

This ideal case with zero reflection at the front (solid line) is compared to the layer stack shown in Fig. 6(a). The layer stack consists of a thick glass layer on top and a 100 nm thick ZnO layer between the glass and the absorber layer. Optically below the absorber are 20 nm ZnO and 300 nm Ag. The glass and the ZnO layers are assumed to be perfectly transparent and the refractive indices for ZnO and Ag are taken from Ref. 76. For the calculation of the absorptance of the layer stack, we used a thin film transfer matrix approach able to calculate absorptances coherently.[77] The difference between the two layer stacks is the angular distribution function of the scattering at the interfaces. While the dotted line represents a layer stack with isotropically scattering surfaces, the dashed line represents flat surfaces. Thus, Fig. 5 shows how much light is lost due to reflections if a realistic layer stack is assumed. This loss is given by the difference between the solid and the dotted line. The current gain due to scattering surfaces and enhanced trapping of weakly absorbed light is given by the difference between the dashed and the dotted line. At $d=300$ nm, the difference due to light trapping amounts to $\Delta J_{sc}\approx 4$ mA/cm^2, which shows that efficient light trapping is a main prerequisite for these thin film approaches.

B. Mobility dependent limits

Up to now, we calculated the SQ limit from the absorption coefficients derived from first principles calculations. In the following, the model described in Sec. II C is used to calculate the radiative limit also for finite mobilities. Compared to the purely optical calculations in the SQ theory, the detailed balance model needs additional parameters, i.e., the mobility and the intrinsic carrier concentration n_i [see Eq. (18)].

The intrinsic carrier concentration follows from the effective density of states N_C and N_V of conduction and valence band and the band gap E_g of the different materials via the equation,

$$n_i = \sqrt{N_C N_V}\exp\left(-\frac{E_g}{2kT}\right). \tag{25}$$

We choose this band gap from the onset of absorption as $E_g(w_{Si}=1.08\ \text{nm})=1.76$ eV, $E_g(w_{Si}=1.62\ \text{nm})=E_g(w_{Si}=2.16\ \text{nm})=1.74$ eV, and $E_g(\text{ZnO/ZnS})=1.88$ eV. The effective DOSs for the superlattices were calculated and are presented in Fig. 7(a). The effective DOS for the nanowire is unknown and was set to an arbitrary value of $N_C=N_V=10^{19}$ cm^{-3}.

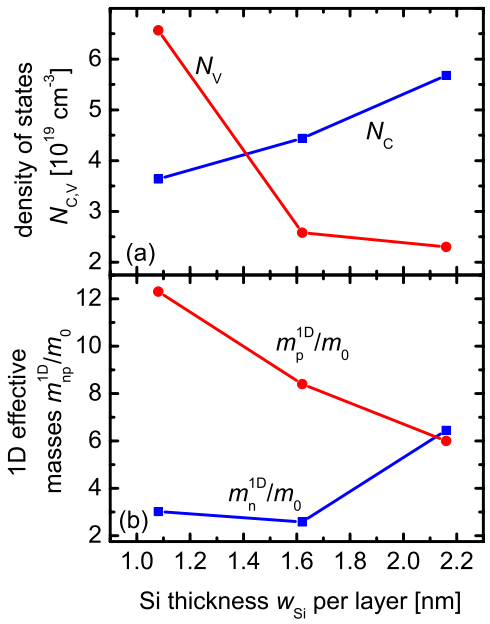

FIG. 7. (Color online) (a) Effective DOS for valence (circles) and conduction band (squares) as well as (b) 1D effective masses normalized to the electron mass in vacuum. The three-dimensional effective DOS follows from the band structure according to Eq. (3). The relation between 1D effective masses and 1D effective DOS is given by Eq. (6). Together with Eq. (26) the effective masses in (b) allow us to calculate the anisotropic electron and hole mobility of the superlattices that are given in Table I.

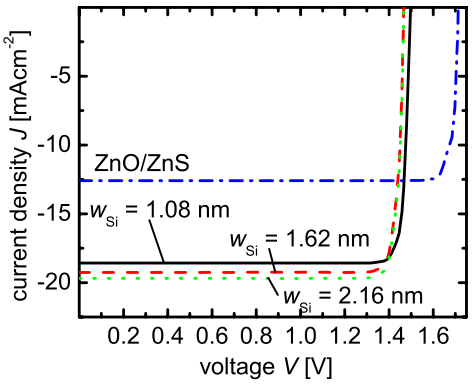

FIG. 8. (Color online) Current/Voltage curves in the radiative high mobility limit for 300 nm thick pin-devices for the four discussed theoretical absorber materials (three SiO_2/Si superlattices: $w_{Si}=1.08$ nm—solid line, $w_{Si}=1.62$ nm—dashed line, $w_{Si}=2.16$ nm—dotted line; and the ZnO/ZnS nanowires—dash-dotted line). The efficiencies from these curves are the same that follow from the calculation of the SQ limit.

This detailed balance model is designed in a way that for high mobilities of free carriers, the result is the same as in the generalized SQ limit. Figure 8 shows the current/voltage curve of the three SiO_2/Si superlattices and the ZnO/ZnS nanowire in the radiative limit and for electron and hole mobilities $\mu_n=\mu_p=10^3$ cm^2(V s)$^{-1}$. The J_{sc}, V_{oc}, and efficiency are equal to those calculated with the radiation balance alone [Eqs. (7)–(11)], thus these mobilities are a good approximation of infinity.

The DOS and the effective masses of electrons and holes are not only relevant to calculate the intrinsic carrier concentration but they have also been used to estimate the mobilities of free charge carriers.[12] The Bloch mobility follows from

$$\mu_{n,p}=\frac{q\tau_{sc}}{m_{n,p}^{1D}}, \tag{26}$$

where τ_{sc} is the scattering time. In case of the SiO_2/Si superlattices the mobility is expected to be strongly anisotropic. Since transport has to take place in the direction normal to the interfaces, the relevant mobility is smaller than the mobility averaged over all directions. Thus we have to determine the 1D effective mass of electrons and holes in z-direction, using Eq. (6). Figure 7(b) shows the result of this calculation normalized to the mass m_0 of electrons in vacuum. In order to calculate mobilities from the effective masses, we still need an estimate of the scattering time τ_{sc}. Jiang and Green[12] discuss this issue extensively for the case of Si quantum dots embedded in a dielectric and we therefore use the same value, namely, $\tau_{sc}=30$ fs. This scattering time together with the effective masses in Fig. 7(b) yields the mobilities $\mu_n=17.6$ cm^2(V s)$^{-1}$, $\mu_p=4.3$ cm^2(V s)$^{-1}$ (for $w_{Si}=1.08$ nm), $\mu_n=20.5$ cm^2(V s)$^{-1}$, $\mu_p=6.3$ cm^2(V s)$^{-1}$ (for $w_{Si}=1.62$ nm), and $\mu_n=8.2$ cm^2(V s)$^{-1}$, $\mu_p=8.8$ cm^2(V s)$^{-1}$ (for $w_{Si}=2.16$ nm).

For the case of the ZnO/ZnS nanowires, we do not have calculations of the effective masses, which are needed to calculate the Bloch mobilities according to Eq. (26). Nevertheless, literature provides values for ZnO nanowires, which are however much thicker than our current nanowires. The reported values are in the range of 10 cm^2(V s)$^{-1}<\mu<30$ cm^2(V s)$^{-1}$.[78–82] Table I summarizes the values for mobility, DOS, and refractive index that we use in the electro-optical simulations. While the DOS and the refractive index are never changed and always correspond to the data presented in Table I, the mobility will be a variable in the

TABLE I. Parameters used for the device simulations if not stated otherwise. The effective DOS and the refractive index are used for Figs. 8–11 and the mobilities for Figs. 10 and 11.

	SiO_2/Si superlattices			ZnO/ZnS nanowires
	$w_{Si}=1.08$ nm	$w_{Si}=1.62$ nm	$w_{Si}=2.16$ nm	
Electron mobility μ_n [cm^2/V s]	17.6	20.5	8.2	10
Hole mobility μ_p [cm^2/V s]	4.3	6.3	8.8	10
Effective density of states for the conduction band N_C [cm^{-3}]	3.64×10^{19}	4.44×10^{19}	5.68×10^{19}	1×10^{19}
Effective density of states for the valence band N_V [cm^{-3}]	6.57×10^{19}	2.58×10^{19}	2.3×10^{19}	1×10^{19}
Index of refraction n	2.37	2.57	2.71	2.5

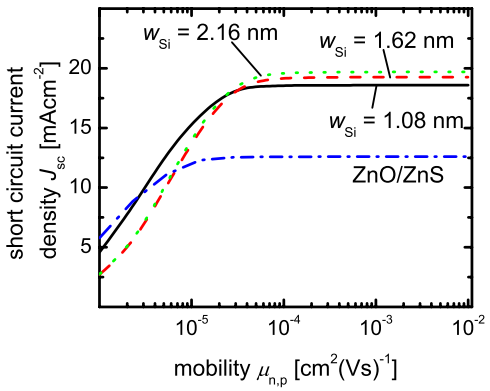

FIG. 9. (Color online) Short circuit current density J_{sc} as a function of electron and hole mobility $\mu=\mu_n=\mu_p$ for the three SiO_2/Si superlattices ($w_{Si}=1.08$ nm—solid line, $w_{Si}=1.62$ nm—dashed line, and $w_{Si}=2.16$ nm—dotted line) and the ZnO/ZnS nanowires (dash-dotted line) in the limit of solely radiative recombination for a pin-type device with a thickness of $d=300$ nm. For mobilities $\mu<10^{-4}$ cm^2/V s, the short circuit current density J_{sc} starts to drop rapidly below its high mobility limit. This critical mobility $\mu_c\approx10^{-4}$ cm^2/V s is around five orders of magnitude below the estimated mobilities, which are in the range of $\mu\approx10^{1}$ cm^2/V s. Thus, we expect mobility to deteriorate device performance only for a considerable amount of nonradiative recombination.

following. Thus, we first ignore the mobilities given in Table I and calculate the radiative limit as a function of mobility.

Figure 9 shows the short circuit current density as a function of the electron and hole mobility in the limit of solely radiative recombination. Here, the mobilities for electrons and holes are assumed to be equal. It is obvious that the critical mobility in the radiative limit is far below the values that have been calculated from the effective masses or have been taken from literature. For all four samples, again with a thickness of $d=300$ nm, the critical mobility μ_c, where the short circuit current starts to drop below its high mobility limit, is in the range 10^{-5} cm^2(V s)$^{-1}<\mu<10^{-4}$ cm^2(V s)$^{-1}$, i.e., 4–6 orders of magnitude below the estimated values. In the following, we need to investigate whether this considerable difference between required and estimated mobilities remains sufficient for high photocurrents also in the case of nonradiative recombination.

C. Nonradiative recombination

The last step from highly idealized devices to more realistic ones is the introduction of nonradiative recombination combined with the inclusion of parasitic absorption in the ZnO window layers. We assume a layer stack as shown in Fig. 6(a) (which is identical to the one used for the calculation of the dashed and dotted lines in Fig. 5) that consists of a thick glass layer on top and a 100 nm thick ZnO layer between the glass and the absorber layer. Optically below the absorber are 20 nm ZnO and 300 nm Ag. The optical properties of the layers are taken from Ref. 79. Taking the same mobilities and DOSs that are given in Table I, we obtain the cell parameters presented in Fig. 10 for the three SiO_2/Si superlattices and for the ZnO/ZnS nanowire as a function of carrier lifetime. Nonradiative recombination is modeled with a recombination rate,

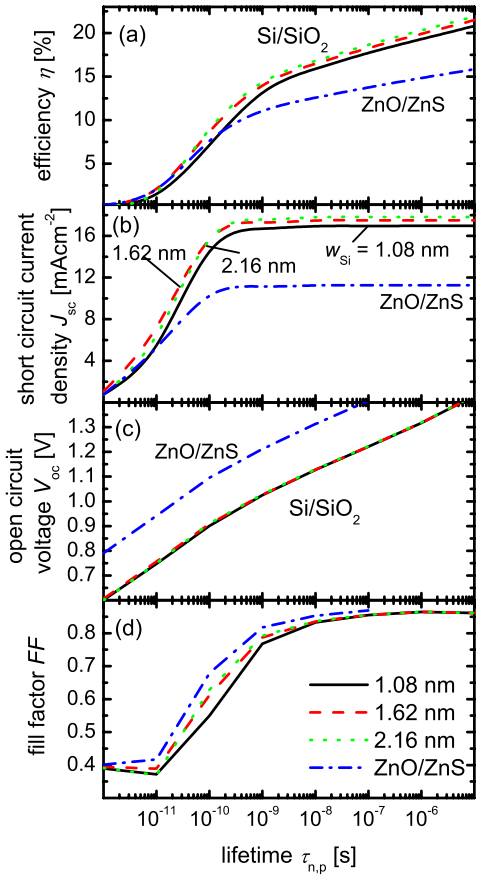

FIG. 10. (Color online) (a) Efficiency, (b) short circuit current density J_{sc}, (c) open circuit voltage V_{oc}, and (d) fill factor FF as a function of electron and hole lifetime $\tau=\tau_n=\tau_p$ for the three SiO_2/Si superlattices ($w_{Si}=1.08$ nm—solid line, $w_{Si}=1.62$ nm—dashed line, and $w_{Si}=2.16$ nm—dotted line) and the ZnO/ZnS nanowires (dash-dotted line). We assume a device thickness of $d=300$ nm and recombination following a SRH statistics with a recombination center in the middle of the device. While the open circuit voltage decreases with shorter lifetimes monotonously with a relatively constant slope, J_{sc} and FF have two regions with a different slope. Above a certain lifetime $\tau>10$ ns (for FF) and $\tau>1$ ns (for J_{sc}), the values are nearly constant, while they drop abruptly for lower lifetimes τ. These critical lifetimes depend linearly on the mobility μ and represent the critical $\mu\tau$ product up to which efficient extraction of the photocurrent is possible.

$$R_{SRH}=\frac{np-n_i^2}{(n+n_i)\tau_p+(p+n_i)\tau_n}, \tag{27}$$

according to Shockley–Read–Hall statistics, where τ_n is the lifetime of electrons and τ_p is the lifetime of holes. In the following, we always set the lifetimes equal, i.e., $\tau_n=\tau_p=\tau$.

Figure 10(a) shows that the efficiency increases monotonically with longer carrier lifetimes τ; however, the curves show two regions with different slopes. For lifetimes $\tau<1$ ns, the increase is steeper than for higher lifetimes. The explanation for that is given by the different dependence of open circuit voltage V_{oc}, fill factor FF, and short circuit current density J_{sc} on the lifetime. Figure 10(b) shows that the short circuit current density J_{sc} stays constant for $\tau>1$ ns and starts to decay drastically when the lifetime drops below 1 ns. In contrast, the slope of the increase in open circuit voltage V_{oc} versus lifetime as shown in Fig. 10(c) does not vary much. The fill factor, which is presented in Fig. 10(d),

follows roughly the decay of the short circuit current density J_{sc}, with the only difference that the drop starts already at slightly longer lifetimes $\tau \approx 10$ ns. This higher sensitivity of the fill factor compared to the short circuit current density J_{sc} to the lifetime is due to the collection of carriers being dependent on the built-in field in the pin-junction. Since the built in field is higher at zero voltage than at maximum power point voltage, the collection at short circuit is more efficient at a given mobility lifetime product $\mu\tau$. With decreasing $\mu\tau$ product, collection at higher voltages and thus the fill factor will therefore suffer already at higher $\mu\tau$ products than the short circuit current density does.

It would now be interesting to estimate the carrier lifetimes one could expect from the superlattice structures and to compare them with the lifetimes required by Fig. 10. In order to calculate surface recombination velocities from lifetime measurements on passivated wafers, Sproul[83] developed an equation for the dependence of lifetime τ_S and surface recombination velocity given by

$$\tau_S = \frac{w}{2S} + \frac{w^2}{D\pi^2}, \tag{28}$$

where w is the thickness of the whole wafer, S is the surface recombination velocity of both surfaces, and D is the minority carrier diffusion constant. If the thickness w decreases, the second term describing the diffusion to the surface vanishes. If we now assume our superlattice to be made up of several Si wells of thickness w that are well passivated with SiO_2, a crude approximation of the resulting lifetime would be to use $\tau_S = w_{Si}/2S$ for the lifetime of a single well and $\tau_S = w_{Si}/(2SN_W)$, where N_W is the number of wells, for a parallel connection of several wells. To estimate the order of magnitude of the lifetime, we assume $w=2$ nm, $S=10$ cm/s representing a very well passivated surface and about 100 wells. This leads to a lifetime of $\tau_S = 100$ ps, which is one or two orders of magnitude below the required lifetimes. It is therefore an important question whether such simplistic calculations are admissible in quantum well solar cells or whether recombination in these devices behaves fundamentally different for extremely small layer thicknesses.

D. Tandem solar cells

The long term goal of research on the presented absorber layers is the use as a top cell in a multijunction solar cell. In order to estimate the usefulness of the SiO_2/Si superlattices for the combination with e.g., crystalline silicon in a two-terminal tandem device, we extended the layer stack used for Fig. 10 by adding a *pn*-junction made of crystalline silicon below the superlattice in pin-configuration. To enhance the photocurrent produced in the top cell, we added a thin, 20 nm thick intermediate reflector layer[84] with the refractive index of SiO_2. Thus, part of the light that hits the back surface of the top cell does not enter the bottom cell, but is reflected back. The thickness of the bottom cell was then chosen in a way that it is as thin as possible, but does not limit the current. Like for the calculations in Fig. 10, we assumed Lambertian light trapping also for the simulation of the tandem cell. The schematic drawing of the assumed layer stack is presented in Fig. 6(b).

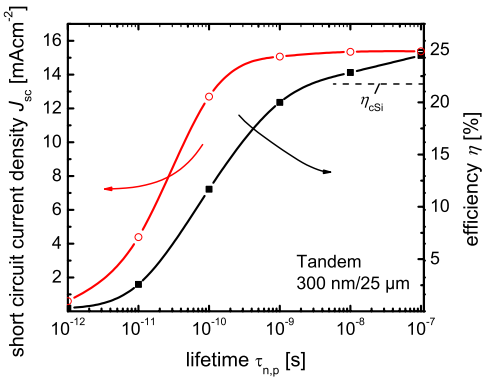

FIG. 11. (Color online) Short circuit current density J_{sc} and efficiency η of a two-terminal tandem cell consisting of a pin-type SiO_2/Si superlattice (Si well thickness $w_{Si}=1.62$ nm, intrinsic layer thickness $d_i=300$ nm) as the top cell and a *pn*-type crystalline silicon bottom cell. The bottom cell thickness of $d_b=25$ μm was chosen such that the bottom cell is not current limiting. The carrier lifetime for the superlattice required for an efficiency of $\eta=20\%$ is roughly $\tau \approx 1$ ns.

Figure 11 shows the short circuit current density and the efficiency of this tandem device as a function of the SRH lifetime of electrons and holes in the top cell. The top cell consists of the SiO_2/Si superlattices with the $w_{Si}=1.62$ nm Si well thickness, since this absorber produced the highest photocurrents in a single junction configuration as shown in Fig. 10. It is obvious that the photocurrent of the tandem device is considerably below the $J_{sc}=21.7$ mA/cm^2 that were identified in Fig. 4 as the optimum value for a *c*-Si based tandem cell. That is due to the fact that the band gap of $E_g=1.74$ eV is close to perfect in the SQ limit for step-functionlike absorptances but not for our more realistic assumptions on device performance. Loss of photocurrent is due to finite absorption coefficients, imperfect light trapping in the tandem configuration (the top cell has no perfect back reflector), nonzero reflection, small amounts of parasitic absorption, and imperfect collection of photogenerated carriers (at least for lifetimes $\tau < 10$ ns). In order to ensure current matching in a two-terminal tandem cell, the band gap of the top cell should therefore be chosen considerably smaller than that given by the band gap in the SQ limit.

The efficiency of the tandem cell just reaches the experimental efficiency limits of crystalline silicon solar cells of $\eta=24.7\%$.[85] Progress beyond that value would need a better adaptation of the two band gaps. However, high efficiencies in the tandem configuration are reached already at a low thickness of the total stack, which is around 25 μm and therefore much thinner than usual wafer-based devices. Due to the difficulties of the top cell to reach a sufficiently high photocurrent, the use of tandem devices will therefore lead to the largest benefit for rather thin and lower quality bottom cells. Note that the efficiency of the *c*-Si bottom cell alone is $\eta=21.8\%$, where we assumed a SRH lifetime $\tau=1$ ms and a surface recombination velocity $S=10$ cm/s.

IV. CONCLUSIONS

We have presented simulations of solar cells consisting of absorber materials that use quantum effects to fine tune

their optical properties. These absorber materials are SiO_2/Si superlattices with different Si well thicknesses and ZnO/ZnS coaxial nanowires. The optical and partly also electrical properties have been obtained by first-principles calculations. Subsequently, these optical and electrical properties have been used to simulate complete devices. To determine meaningful efficiency limits we have gone step by step from idealized systems as defined by the SQ theory to more realistic systems, where the efficiency limits are, however, less fundamental. These device simulations allow us to determine critical values for device properties as mobility and carrier lifetime that must be met to ensure efficient photovoltaic energy conversion. Simulations of complete tandem devices show that there is a considerable difference in photocurrent between the SQ theory and more realistic simulations. To ensure current matching albeit this difference in photocurrent one needs considerably lower band gaps for the top cell, thereby increasing the part of the spectrum absorbed by the top cell.

ACKNOWLEDGMENTS

The authors are grateful for support by the German Ministry for Education and Research (BMBF) (Contract Nos. 03SF0308 and 13N9669). The authors would like to thank J. Schrier (Haverford College) for providing the absorption coefficients for the ZnO/ZnS nanowires. The authors would also like to thank J. Mattheis (Solsol GmbH) for fruitful discussions and U. Gösele (MPI Halle) for reading the manuscript.

[1] D. E. Carlson and C. R. Wronski, Appl. Phys. Lett. **28**, 671 (1976).
[2] D. M. Chapin, C. S. Fuller, and G. L. Pearson, J. Appl. Phys. **25**, 676 (1954).
[3] S. Wagner, J. L. Shay, and H. M. Kasper, Appl. Phys. Lett. **25**, 434 (1974).
[4] J. L. Shay, S. Wagner, and H. M. Kasper, Appl. Phys. Lett. **27**, 89 (1975).
[5] D. Ginley, M. A. Green, and R. Collins, MRS Bull. **33**, 355 (2008).
[6] M. A. Green, Prog. Photovoltaics **9**, 123 (2001).
[7] M. A. Green, *Third Generation Photovoltaics* (Springer, Berlin, 2003).
[8] N. S. Lewis, Science **315**, 798 (2007).
[9] R. F. Service, Science **319**, 718 (2008).
[10] W. Shockley and H. J. Queisser, J. Appl. Phys. **32**, 510 (1961).
[11] U. Aeberhard and R. H. Morf, Phys. Rev. B **77**, 125343 (2008).
[12] C.-W. Jiang and M. A. Green, J. Appl. Phys. **99**, 114902 (2006).
[13] Ch. Kittel, *Introduction to Solid State Physics* (Wiley, New York, 2005).
[14] R. Enderlein and N. J. M. Horing, *Fundamentals of Semiconductor Physics and Devices* (World Scientific, Singapore, 1997).
[15] T. Tiedje, E. Yablonovitch, G. C. Cody, and B. G. Brooks, IEEE Trans. Electron Devices **31**, 711 (1984).
[16] K. Seino, J.-M. Wagner, and F. Bechstedt, Appl. Phys. Lett. **90**, 253109 (2007).
[17] J. Schrier, D. O. Demchenko, L.-W. Wang, and A. P. Alivisatos, Nano Lett. **7**, 2377 (2007).
[18] M. A. Green, K. Emery, Y. Hisikawa, and W. Warta, Prog. Photovoltaics **15**, 425 (2007).
[19] F. Dimroth and S. Kurtz, MRS Bull. **32**, 230 (2007).
[20] T. Trupke, M. A. Green, and P. Würfel, J. Appl. Phys. **92**, 4117 (2002).
[21] A. Shalav, B. S. Richards, T. Trupke, K. W. Kramer, and H. U. Gudel, Appl. Phys. Lett. **86**, 013505 (2005).
[22] T. Trupke, M. A. Green, and P. Würfel, J. Appl. Phys. **92**, 1668 (2002).
[23] D. Timmerman, I. Izeddin, P. Stallinga, I. N. Yassievich, and T. Gregorkiewicz, Nat. Photonics **2**, 105 (2008).
[24] R. T. Ross and A. J. Nozik, J. Appl. Phys. **53**, 3813 (1982).
[25] P. Würfel, Sol. Energy Mater. Sol. Cells **46**, 43 (1997).
[26] M. Neges, K. Schwarzburg, and F. Willig, Sol. Energy Mater. Sol. Cells **90**, 2107 (2006).
[27] A. J. Nozik, Physica E **14**, 115 (2002).
[28] V. I. Klimov, J. Phys. Chem. B **110**, 16827 (2006).
[29] P. Guyot-Sionnest, Nature Mater. **4**, 653 (2005).
[30] R. D. Schaller, M. Sykora, J. M. Pietryga, and V. I. Klimov, Nano Lett. **6**, 424 (2006).
[31] R. J. Ellingson, M. C. Beard, J. C. Johnson, P. Yu, O. I. Micic, A. J. Nozik, A. Shabaev, and A. L. Efros, Nano Lett. **5**, 865 (2005).
[32] R. D. Schaller, V. A. Agranovich, and V. I. Klimov, Nat. Phys. **1**, 189 (2005).
[33] G. Nair and M. G. Bawendi, Phys. Rev. B **76**, 081304(R) (2007).
[34] F. Meillaud, A. Shah, C. Droz, E. Vallat-Sauvain, and C. Miazza, Sol. Energy Mater. Sol. Cells **90**, 2952 (2006).
[35] G. Conibeer, M. A. Green, R. Corkish, Y. Cho, E.-C. Cho, C.-W. Jiang, T. Fangsuwannarak, E. Pink, Y. Huang, T. Puzzer, T. Trupke, B. Richards, A. Shalav, and K. Lin, Thin Solid Films **511-512**, 654 (2006).
[36] G. Conibeer, M. A. Green, E.-C. Cho, D. König, Y.-H. Cho, T. Fangsuwannarak, G. Scardera, E. Pink, Y. Huang, T. Puzzer, S. Huang, D. Song, C. Flynn, S. Park, X. Hao, and D. Mansfield, Thin Solid Films **516**, 6748 (2008).
[37] T. Mchedlidze, T. Arguirov, S. Kouteva-Arguirova, M. Kittler, R. Rölver, B. Berghoff, D. L. Bätzner, and B. Spangenberg, Phys. Rev. B **77**, 161304 (2008).
[38] R. Rölver, B. Berghoff, D. L. Bätzner, B. Spangenberg, and H. Kurz, Appl. Phys. Lett. **92**, 212108 (2008).
[39] B. Stegemann, A. Schöpke, and M. Schmidt, J. Non-Cryst. Solids **354**, 2100 (2008).
[40] L. Van Dao, J. Davis, P. Hannaford, Y.-H. Cho, M. A. Green, and E.-C. Cho, Appl. Phys. Lett. **90**, 081105 (2007).
[41] D. Song, E.-C. Cho, G. Conibeer, Y. Huang, and M. A. Green, Appl. Phys. Lett. **91**, 123510 (2007).
[42] D. Song, E.-C. Cho, G. Conibeer, Y. Huang, C. Flynn, and M. A. Green, J. Appl. Phys. **103**, 083544 (2008).
[43] C. Meier, A. Gondorf, S. Lüttjohann, A. Lorke, and H. Wiggers, J. Appl. Phys. **101**, 103112 (2007).
[44] T. Kirchartz and U. Rau, Thin Solid Films **516**, 7144 (2008).
[45] G. Kresse and J. Furthmüler, Comput. Mater. Sci. **6**, 15 (1996).
[46] G. Kresse and D. Joubert, Phys. Rev. B **59**, 1758 (1999).
[47] L. E. Ramos, J. Furthmüller, and F. Bechstedt, Phys. Rev. B **69**, 085102 (2004).
[48] J.-M. Wagner, K. Seino, F. Bechstedt, A. Dymiati, J. Mayer, R. Rölver, M. Först, B. Berghoff, B. Spangenberg, and H. Kurz, J. Vac. Sci. Technol. A **25**, 1500 (2007).
[49] N. Tit and M. W. C. Dharma-wardana, Phys. Lett. A **254**, 233 (1999).
[50] W. G. Aulbur, L. Jönsson, and J. W. Wilkins, Solid State Phys. **54**, 1 (2000).
[51] K. Seino and F. Bechstedt, in preparation.
[52] B. Adolph, V. I. Gavrilenko, K. Tenelsen, F. Bechstedt, and R. Del Sole, Phys. Rev. B **53**, 9797 (1996).
[53] P. Würfel, J. Phys. C **15**, 3967 (1982).
[54] M. Planck, *Vorlesungen über die Theorie der Wärmestrahlung* (Barth, Leipzig, 1906).
[55] G. Kirchhoff, Ann. Phys. **109**, 275 (1860).
[56] C. H. Henry, J. Appl. Phys. **51**, 4494 (1980).
[57] A. Martí and G. L. Araújo, Sol. Energy Mater. Sol. Cells **43**, 203 (1996).
[58] P. Campbell and M. A. Green, J. Appl. Phys. **62**, 243 (1987).
[59] S. Fahr, C. Rockstuhl, and F. Lederer, Appl. Phys. Lett. **92**, 171114 (2008).
[60] C. Rockstuhl, F. Lederer, K. Bittkau, and R. Carius, Appl. Phys. Lett. **91**, 171104 (2007).
[61] E. Yablonovitch, J. Opt. Soc. Am. **72**, 899 (1982).
[62] S. Fahr, C. Ulbrich, T. Kirchartz, U. Rau, C. Rockstuhl, and F. Lederer, Opt. Express **16**, 9332 (2008).
[63] J. Mattheis, Mobility and Homogeneity Effects on the Power Conversion Efficiency of Solar Cells, Ph.D. thesis (University of Stuttgart, 2008), p. 140.
[64] T. Kirchartz, A. Helbig, and U. Rau, Sol. Energy Mater. Sol. Cells **92**, 1621 (2008).
[65] C. Ulbrich, S. Fahr, J. Üpping, M. Peters, T. Kirchartz, C. Rockstuhl, R. Wehrspohn, A. Gombert, F. Lederer, and U. Rau, Phys. Status Solidi A, **205**, 2831 (2008).
[66] P. W. Bridgman, Phys. Rev. **31**, 101 (1928).
[67] G. N. Lewis, Proc. Natl. Acad. Sci. U.S.A. **11**, 179 (1925).
[68] R. C. Tolman, Proc. Natl. Acad. Sci. U.S.A. **11**, 436 (1925).
[69] O. E. Richardson, Proc. R. Soc. London **36**, 392 (1924).
[70] E. O. Lawrence, Phys. Rev. **27**, 555 (1926).

[71]T. Kirchartz and U. Rau, Phys. Status Solidi A **205**, 2737 (2008).
[72]T. Kirchartz, J. Mattheis, and U. Rau, Phys. Rev. B **78**, 235320 (2008).
[73]A. Martí, J. L. Balenzategui, and R. F. Reyna, J. Appl. Phys. **82**, 4067 (1997).
[74]J. Mattheis, J. H. Werner, and U. Rau, Phys. Rev. B **77**, 085203 (2008).
[75]W. van Roosbroeck and W. Shockley, Phys. Rev. **94**, 1558 (1954).
[76]M. Zeman, R. A. C. M. M. van Swaaij, J. W. Metselaar, and R. E. I. Schropp, J. Appl. Phys. **88**, 6436 (2000).
[77]M. Zeman, J. van den Heuvel, B. E. Pieters, M. Kroon, and J. Willemen, *Advanced Semiconductor Analysis* (TU Delft, The Netherlands, 2003).
[78]J. B. Baxter and C. A. Schmuttenmaer, J. Phys. Chem. B **110**, 25229 (2006).
[79]K. Keem, D.-Y. Jeong, S. Kim, M.-S. Lee, I.-S. Yeo, U.-I. Chung, and J.-T. Moon, Nano Lett. **6**, 1454 (2006).
[80]Y. Liu, Z. Y. Zhang, Y. F. Hu, C. H. Jin, and L.-M. Peng, J. Nanosci. Nanotechnol. **8**, 252 (2008).
[81]Y.-Y. Noh, X. Cheng, H. Sirringhaus, J. I. Sohn, M. E. Welland, and D. J. Kang, Appl. Phys. Lett. **91**, 043109 (2007).
[82]D.-I. Suh, S.-Y. Lee, J.-H. Hyung, T.-H. Kim, and S.-K. Lee, J. Phys. Chem. C **112**, 1276 (2008).
[83]A. B. Sproul, J. Appl. Phys. **76**, 2851 (1994).
[84]P. Buehlmann, J. Bailat, D. Domine, A. Billet, F. Feltrin, and C. Ballif, Appl. Phys. Lett. **91**, 143505 (2007).
[85]J. Zhao, A. Wang, M. A. Green, and F. Ferrazza, Appl. Phys. Lett. **73**, 1991 (1998).